Subduction zone and carbonate platform interactions since the Devonian: influence on palaeo-atmospheric CO_2 and the deep carbon cycle

Jodie Pall[1], Sabin Zahirovic[1], Sebastiano Doss[1], Rakib Hassan[1,2], Kara J. Matthews[1,3], John Cannon[1], Michael Gurnis[4], Louis Moresi[5], Adrian Lenardic[6] and R. Dietmar Müller[1]

[1]EarthByte Group, School of Geosciences, University of Sydney, NSW 2006, Australia.
[2]Geoscience Australia, GPO Box 378, Canberra 2601, ACT, Australia.
[3]Department of Earth Sciences, University of Oxford, Oxford, OX1 3AN, UK.
[4]Seismological Laboratory, California Institute of Technology, California 91125, USA.
[5]School of Earth Sciences, University of Melbourne, Victoria 3010, Australia.
[6]Department of Earth Science, Rice University, Texas 77005, USA.

Correspondence to: Jodie Pall (jodierae.pall@gmail.com)

Abstract

The CO_2 liberated along continental subduction zones through intrusive/extrusive magmatic activity and the resulting active and diffuse outgassing influences global atmospheric CO_2. However, when melts derived from continental subduction zones intersect buried carbonate platforms, decarbonation reactions may cause the contribution to atmospheric CO_2 to be far greater than segments of the active margin that lacks buried carbon-rich rocks and carbonate platforms. This study investigates the contribution of carbonate-intersecting continental (CIC) subduction zones to palaeo-atmospheric CO_2 levels over the past 410 million years by integrating a plate motion and plate boundary evolution model with carbonate platform development through time.

Continuous and cross-wavelet analyses as well as wavelet coherence are used to evaluate trends between the evolving lengths of CIC subduction zones, non-CIC subduction zones and total global subduction zones, and are examined for periodic, linked behaviour with the proxy-CO_2 record between 410 Ma and the present. Wavelet analysis reveals significant linked periodic behaviour between 75-50 Ma, where CIC subduction zone lengths are relatively high and are correlated with peaks in palaeo-atmospheric CO_2, characterised by a ~32 Myr periodicity and a 10 Myr lag of CO_2 peaks following CIC subduction zone

length peaks. The linked behaviour may suggest that the relative abundance of CIC subduction zones played a role in affecting global climate during the Late Cretaceous to Early Palaeogene greenhouse. At all other times, atmospheric CO_2 emissions from CIC subduction zones are not well correlated with the proxy-CO_2 record. Our analysis of reconstructed carbonate platforms in relation to continental subduction zones does not support the idea that CIC subduction zone activity is more important than non-CIC subduction zone activity in driving changes in palaeo-atmospheric CO_2 levels. This suggests that carbon fluxes from subduction zones and carbonate platform intersections are time-varying and that other feedback mechanisms between the geosphere, atmosphere and biosphere likely play dominant roles in modulating climate since the Devonian. Our modelled subduction zone lengths and carbonate-intersecting arc lengths approximate magmatic activity through time, and can be used as input into fully-coupled models of CO_2 flux between deep and shallow carbon reservoirs.

1 Introduction

The current paradigm of the deep carbon cycle (i.e. the planetary cycling of carbon over million-year timescales) attributes fluctuations in the atmospheric carbon dioxide (CO_2) to the realm of tectonic forces, where subduction-related emissions (van der Meer et al., 2014; Kerrick, 2001) and metamorphic decarbonation (Lee et al., 2013) are major CO_2 sources, and the processes of silicate weathering (Sundquist, 1991; Kent and Muttoni, 2008) and marine organic carbon burial (Berner and Caldeira, 1997; Ridgwell and Zeebe, 2005) are major sinks removing CO_2 from the atmosphere. Subduction plays a critical role in this cycle. In a dynamic interplay, oceanic lithosphere is consumed at subduction zones, removing carbon bound in pelagic carbonate seafloor sediments from the exogenic carbon cycle. Simultaneously, CO_2 is emitted through diffuse outgassing and arc volcanism along subduction zones (Keleman and Manning, 2015). Despite the proposal that silicate weathering has, at some stages, been a dominating control of atmospheric CO_2 levels (Kump, 2000; Kent and Muttoni, 2013), arc magmatism at icehouse-greenhouse transitions is thought to be the first-order control on climate fluctuations while silicate weathering acts to modulate atmospheric CO_2 as a secondary regulative process (Ridgwell and Zeebe, 2005; Lee and Lackey, 2015; McKenzie et al., 2016). Recent studies have found support for links between global arc activity and icehouse-greenhouse transitions using detrital zircon ages, modelling and

experimental techniques, particularly as drivers of greenhouse conditions in the Cambrian (McKenzie et al., 2016; Cao et al., 2017), Jurassic-Cretaceous (McKenzie et al., 2016) and early Palaeogene (Lee et al., 2013; Carter and Dasgupta, 2015; Cao et al., 2017).

Recently, carbon and helium isotope analysis from modern volcanic arc gas has provided evidence that volcanic arcs that assimilate crustal carbonate in their magmas through decarbonation reactions have a greater atmospheric CO_2 contribution than other types of arcs (Mason et al., 2017). Modern crustal carbonate reservoirs are a result of global organic and inorganic carbonate production throughout the Phanerozoic, which has contributed to the build-up of expansive, shallow-water carbonate sequences including ramps and rimmed shelves along continental margins, hereafter referred to as 'carbonate platforms' (Kiessling et al., 2003). At different points in Earth's history, active (from extrusive volcanism) and passive (from intrusive magmatism) emissions from carbonate-intersecting continental (CIC) subduction zones may have dominated global carbon flux from subduction zones, such as during the Cretaceous (144-65 Ma) where continental arcs are hypothesised to have been longer than modern day lengths and where a greenhouse climate prevailed (Lee et al., 2013; van der Meer et al., 2014; Cao et al., 2017). It is plausible that at other points in Earth's history, crustally-derived carbon has played a significant role in affecting global climate, and that there may be a periodic trend in carbon released from continental arcs through time related to ~50 Myr flare-ups (Lee and Lackey, 2015) and continent assembly and dispersal which cause transitions from intraoceanic-arc- to continental-arc-dominated states (Lenardic et al., 2011; Lee et al. 2013). However, it is difficult to test this hypothesis, especially due to due to poor preservation of ancient intra-oceanic arc rocks (Berner, 2004).

This challenge is addressed using wavelet analysis, which attempts to detect correlations and periodicities in two time series at any scale or duration (Grinsted et al., 2004). Compared to other windowing techniques that find time-dependent correlations between two signals such as the windowed Fourier transform, the wavelet transform is preferable because it is localised (bounded) in both time and frequency, whereas Fourier transforms are only localised in frequency (Torrence and Compo, 1998). Hence, the wavelet transform can better constrain correlations in time and is better-suited than the Fourier transform to approximating data with sharp discontinuities, such as those addressed in this investigation.

We aim to investigate whether the CO_2 flux from CIC subduction zones is significantly different to the flux from subduction zones that do not intersect with buried carbonate reservoirs (non-CIC) in influencing global palaeo-atmospheric CO_2 concentrations. Our study explores volcanic and passive outgassing of CO_2 along continental subduction zones as an aspect of the deep Earth carbon cycle using a combination of plate reconstruction software and wavelet analysis. Only Cao et al. (2017) and this study have endeavoured to apply palaeogeographic maps to explore the distribution of continental arcs through space and time in a plate tectonic framework. However, the work by Cao et al. (2017) relies on discrete plate reconstruction snapshots, rather than the continuously evolving plate boundary evolution model applied here. In addition, Cao et al. (2017) compile arc volcanic products, which may be affected by preservation and sampling bias, and may not capture magmatic products trapped (deep) in the crust or those lost to erosion. The Cao et al. (2017) approach of estimating continental subduction zone lengths is therefore a lower-limit, while our approach is likely an upper limit of continental subduction zone lengths through time. Furthermore, wavelet analysis is used to deconcolve two time series at a time (e.g. our CIC and non-CIC subduction zone lengths with the palaeo-atmospheric CO_2 record by Park and Royer [2011]) to uncover any periodicities or correlations. With a plate motion model that extends to 410 Ma, we track space-time trends of global subduction zone and carbonate platform interactions since the Devonian. This paper is accompanied by an open-source 'subduction zone analysis toolkit' (Doss et al., 2016) to help enable the use of digital plate motion models (e.g. Matthews et al., 2016) and other tools to investigate aspects of the deep carbon cycle.

2 Modelling subduction zones evolution

We investigate the combined effect of evolving global subduction zone lengths and the subsequent decarbonation of crustal carbonates by subduction zone melts to create a first-order approximation of the contribution of CO_2 outgassed at carbonate-intersecting continental (CIC) subduction zones to palaeo-CO_2 levels over the past 410 Myr. An 'Accumulation Model' of carbonate platform evolution was produced to represent the long-term persistence and build-up of carbonate platforms in upper continental crust. The plate reconstructions used in this study have been developed through a synthesis of marine and continental geological and geophysical data, including seafloor spreading

histories for the post-Pangea timeframe (Seton et al., 2012; Muller et al., 2016), and largely paleomagnetic and continental geological constraints for pre-Pangea times (Domeier and Torsvik, 2014; Matthews et al., 2016). Continental subduction zones are implemented where the geological record indicates arc volcanism or intrusive magmatism, an active accretionary melange, active orogens associated with subduction zones, formation of supra-subduction zone ophiolites, and other indicators of an active margin. As our plate reconstructions are global, plate boundary evolution requires continuously evolving topological polygons to capture plate motions (Gurnis et al., 2012), meaning that subduction zones are implemented along entire convergent margins, rather than only where preserved arc volcanics are found. Our plate reconstructions that include continental motions and plate boundary evolution are available as open-access community resources (https://www.earthbyte.org/global-plate-models/).

2.1 An 'Accumulation' model of carbonate platform development

Palaeogeographic maps of carbonate platforms spanning the Phanerozoic since the Ordovician from Kiessling et al. (2003) were used to model carbonate platform accumulation through time. The 31 maps represent the spatial extent of carbonate platforms at the maximum marine transgression within each epoch for the Phanerozoic (Kiessling et al., 2003). The carbonate platform geometries were georeferenced to WGS84 co-ordinates in ArcGIS (ESRI, 2011) to be compatible with GPlates, the open-source plate reconstruction software (Boyden et al., 2011). A GPlates file was created to depict carbonate platform accumulation from 410 Ma to present-day using platforms existing since the Ordovician, in order to better capture buried carbonate platforms at the beginning of the model timeframe. Creating this model involved stitching together all carbonate platform shapefiles and allowing them to persist until present day. Ages had been ascribed based on the Golonka and Kiessling (2002) Phanerozoic timescale. However, owing to new chronostratigraphic data, the geological times ascribed to the existence of carbonate platforms in each epoch were converted to the corresponding times in the latest chronostratigraphic scheme given in the 2016 version of the International Stratigraphic Chart (Cohen et al., 2013). Subsequently, the static carbonate platform shapefiles were reconstructed with the rotations and plate geometries associated with an older plate motion model (Scotese, 2016), similar to the model used by Kiessling et al. (2003). In

GPlates, the carbonate platform geometries were assigned Plate IDs based upon their overlapping position within the reconstructed continental geometry. Carbonate platforms were rotated to their present-day positions, and Plate IDs associated with the Scotese (2016) model were translated into corresponding Plate IDs from the Matthews et al. (2016) plate motion model. By obtaining the present-day geometry of the ancient carbonate platforms, attaching these geometries to any other plate motion model becomes straightforward. The evolving carbonate platform model was created by layering each carbonate platform geometry such that it persists to present-day. The 'Accumulation' Model we implement in this study embodies the idea that carbonate platforms accumulate in crustal reservoirs through time.

W

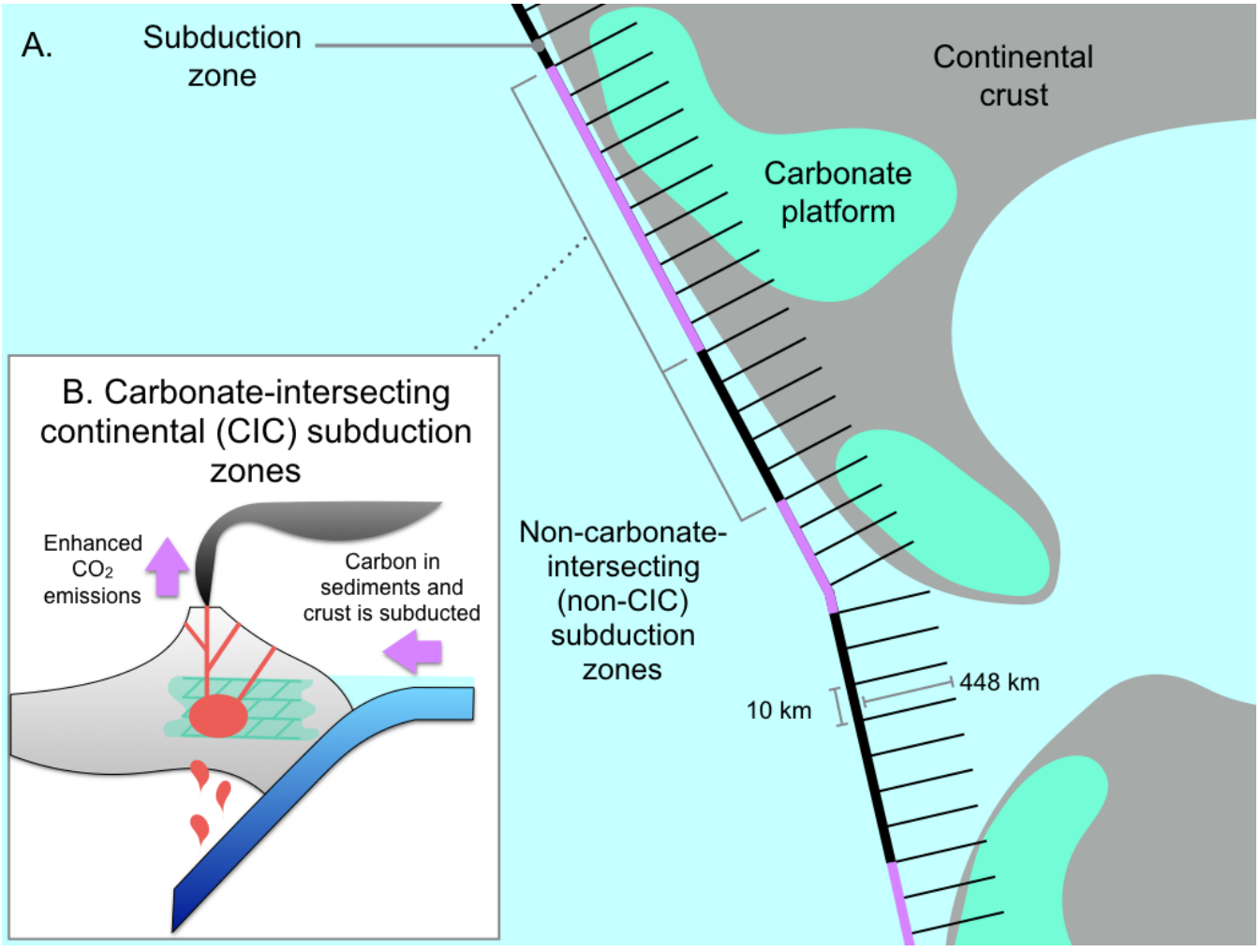

Figure 1: (A) Schematic representation of the ~450-km-long cross-profile 'whiskers' that were constructed along subduction zones (purple and black) spaced 10 km apart in the direction of subduction. At regular intervals along the whiskers, the carbonate platform grid on the overriding plate was sampled where carbonate polygons have a value of 1, and everywhere else is zero. If the whisker intersects with a carbonate platform, it represents 10 km along a carbonate-intersecting volcanic arc. (B) Schematic representations of carbonate-intersecting continental arcs. Carbonate platforms become buried over time, forming reservoirs in the crust. Through assimilation and decarbonation reactions, arc magmas interact with upper-crustal carbonates and liberate significantly more CO_2 emissions that at non-intersecting continental arcs.

2.2 Assumptions and limitations of the Accumulation Model

The Accumulation Model is an end-member scenario of how carbonate platforms evolve through time. Carbonate accumulation is assumed to accrete on continental margins and persist as mid-crustal carbonate reservoirs from the time of their formation to the present (Fig. 1). Ancient carbonate platforms are known to persist to present-day in surface reservoirs, and can be reconstructed from the geological record as they either outcrop, are sampled by drilling or are interpreted from seismic reflection studies (Kiessling et al., 2003). Some crustal carbonate is inevitably eroded or subducted into the deep mantle, however it is improbable that most reservoirs have been destroyed in this way as most carbonate platforms accumulate on continental margins and are not likely to subduct (Lee and Lackey, 2015). Given limited erosion on passive continental margins, except in the cases of major uplift and deformation through mountain-building, it is far more likely that carbonate platform accretion has exceeded their depletion by erosion or consumption through time (Ridgewell and Zeebe, 2005). Moreover, the existence of fossil reef data as far back as the Precambrian (Grotzinger and James, 2000) favours the notion that extensive portions of platforms have been well-preserved in continents.

Nevertheless, our model assumes that carbonate platforms have not been significantly depleted by sustained mantle-crust interaction through time. We follow this assumption because there is no way to account for their rate of depletion given the complexity of inter-dependent factors such as platform thickness, heat, pressure, composition and the duration of interaction (Johnston et al., 2011). Accounting for the thickness of platforms and the depletion of reservoirs over time are areas of necessary future developments in the model. We accept that our Accumulation Model is a simplification of the carbonate reservoir system and may lead to an overestimation of CIC subduction zone lengths. However, this may be a reasonable proxy for the substantial amount of CO_2 emitted via diffuse outgassing that is largely unaccounted for in global estimates of carbon emitted at continental arcs (fore-arc, arc and back-arc settings) (Keleman and Manning, 2015). Given little evidence of carbon storage in arc crust, these

estimates provide important information, if not an upper-bound estimate, of degassing from CIC subduction zones which are hypothesised to be a significant source of atmospheric CO_2 (Keleman and Manning, 2015). While some Precambrian carbonate platforms have been described (Grotzinger and James, 2000), no effort has yet been made to map their occurrence globally, and thus only those captured in the Kiessling et al. (2003) biogeographic maps could be incorporated into our Accumulation Model. While it is expected that accounting for Precambrian platforms would not drastically change the analysis, this model nevertheless represents a degree of underestimation of the crustal carbonate reservoir.

2.3 Measuring global subduction zone lengths with pyGPlates

We use the open access global plate motion model from Matthews et al. (2016) to analyse the spatio-temporal distribution of subduction zone volcanic arcs in a deep-time tectonic framework and test the hypothesis that subduction zone arc lengths are correlated with atmospheric CO_2 levels. The model spans much of the Phanerozoic as it links the 410-250 Ma Domeier and Torsvik (2014) and the 230-0 Ma Müller et al. (2016) plate motion models. Using open-source and cross-platform plate reconstruction software GPlates (http://gplates.org/download.html) and a new pyGPlates Python application programming interface (API) (https://www.gplates.org/docs/pygplates/), we measure the length of subduction zones at 1 Myr intervals since 410 Ma and track the length of subduction zones that interact with carbonate platforms (CIC subduction zones) from the Kiessling et al. (2003) compilation, the length of all subduction zones that do not intersect carbonate platforms (non-CIC subduction zones), and total global subduction zone lengths. Using the pyGPlates workflow (Doss et al., 2016), global subduction zone boundaries were extracted from the Matthews et al. (2016) plate motion model, and subduction zone geometries were adjusted to remove any overlapping line segments that would overestimate arc lengths through time.

2.4 Computing the intersections of carbonate platforms and subduction zones

We test whether continental subduction zones interacting with carbonate platforms are different from non-intersecting portions of subduction zones in their contribution to global atmospheric CO_2 concentrations, and hence we track the lengths of subduction zones that both do and do not intersect with

carbonate platforms in the overriding continental crust. Carbonate platform geometries were converted to polygons using *grdmask* from the development version of Generic Mapping Tools (GMT) (v.5.2.1; Wessel et al., 2015) which created a Boolean-style mask consisting of closed domains with a value of 1 where carbonate platforms existed and 0 elsewhere. We identified polygons proximal to subduction boundaries through time using the exported subduction zone geometries from the pyGPlates workflow. We compute the signed-distance function, positive toward the overriding plate, on the surface of the sphere for all subduction zones and computed where the carbonate platforms lie within +448 km of the trench. The *grdtrack* tool in GMT was used to create large tracks of ~450 km-long cross-profiles perpendicular to subduction boundaries at a uniform spacing of 10 km, with 'whiskers' pointing in the direction of subduction (Fig. 1a). The whiskers had five evenly-spaced nodes to detect intersections with carbonate platform polygons. We determined the ~450 km-long inclusion distance by determining average arc-trench distances using the present-day 'Volcanoes of the World' database maintained by the Smithsonian Institution's Global Volcanism Program (Siebert and Simkin, 2014). From a sample size of 1023 volcanoes, average arc-trench distances are 287 km with a standard deviation of 161 km, which gives an upper estimate distance of 448 km. This captures ~84% of the location of all volcanic arcs and corresponds to an upper limit for interactions with volcanic arcs in our assumptions. The whiskers function as a buffer, allowing us to identify the lengths of subduction zone boundaries within ~450 km perpendicular radius of a carbonate platform polygon. Cross-profiles that overlap with carbonate platform polygons demarcate areas where continental subduction zones interact with crustal carbonates (Fig. 1b). Due to the complexity and time-variability of subduction, we do not consider times during which flat slab subduction may have occurred, which would result in greater arc-trench distances and is beyond the scope of this study.

3 Linking arc volcanism to palaeoclimate change

Relationships between oscillations in two time-series can be examined using a wavelet analysis to elucidate the scales and time intervals where the proxy record and modelled data display correlated, periodic signals. We performed wavelet analysis as a means of identifying localised variations of power between proxy records of CO_2 and modelled CIC subduction zone lengths and in turn

investigate the temporal evolution of these aperiodic signals. We are able to carry out this analysis as the geophysical data exhibit non-stationarity; dominant periodic signals vary in their frequency and amplitude through time. The continuous wavelet transform (CWT) is particularly useful for this task as it better characterises oscillatory behaviours of signals than discrete wavelet transforms. The CWT was applied to decompose arc lengths and proxy signals into time and frequency space simultaneously using functions (wavelets) that vary in width to discern both the high and low frequency features present (Lau and Weng, 1995; Supplement 3). To examine whether trends in atmospheric CO_2 and carbonate-intersecting arcs are connected in some way, the cross-wavelet transform (XWT) was carried out between the proxy-CO_2 data (Fig. S1) and each of the modelled data on carbonate-intersecting arc lengths (Supplement 4). The XWT reveals space-time regions where the two datasets coincidentally have high common power as well as calculating the phase relationships between signals, indicating where two series co-vary (Grinsted et al., 2004). Wavelet coherence (WTC) is computed in tandem with the XWT and determines if the time series are significantly interrelated in the frequency domain. All wavelet analysis was carried out for each detrended and filtered time series using the Wavelet Coherence Toolbox™ for MATLAB® based on the statistical approach applied to geological and geophysical data by Torrence and Compo (1998) and Grinsted et al. (2004).

3.1 Data filtering

The modelled results and proxy-CO_2 time series were pre-processed for wavelet analysis by detrending and applying a low-pass filter using MATLAB®'s Signal Processing Toolbox™. The proxy-CO_2 time series is non-uniformly distributed with multiple data values at certain time steps. Prokoph and Bilali (2008) stress the importance of keeping a consistent time-scale across all time-series when examining causation between trends. Therefore, the data were first processed so that the median atmospheric CO_2 (ppm) value was taken at all time steps with multiple observations (Fig. S1). The data were then resampled with the MATLAB *resample* function to have 410 uniformly spaced data points across the 410 Myr timeframe. The function interpolates the time series linearly, and the series was found to be relatively insensitive to the interpolation method used. A moving average filter was applied using

the MATLAB *filter* function with a window size of 7 Myr to remove high-frequency signals that may represent noise or other short-term perturbations (Fig. S2). In the time-frequency domain, our focus is on the power in the mid-to-high frequency spectrum and so the moving average filter was designed to remove periods less than 5 Myrs. As a result, the analysis does not capture any geologically-rapid (few Myrs) changes in CO_2 that may be driven by changes in plate tectonics and carbonate platform-arc interactions.

Rather than comparing estimates from the Accumulation Model with Phanerozoic atmospheric CO_2 models like COPSE (Bergman et al., 2004) or GEOCARBSULF (Berner, 2006), results were compared to the proxy-CO_2 record compiled by Park and Royer (2011) because the unresolved uncertainties in model calculations may have rendered comparisons less meaningful than when comparing with proxy records. The proxy-CO_2 dataset presented by Park and Royer (2011) is an expanded version of the Royer (2006) collection, which originally incorporated data from 490 sources from the Phanerozoic (542 Ma to present) to present including palaeosols, foraminifera, stomatal indices, $\delta^{11}B$ in marine carbonates and the $\delta^{13}C$ of liverworts. The collection was chosen as it is the most up-to-date proxy-CO_2 data with the highest temporal resolution available.

4 Results

4.1 Continuous Wavelet Transform (CWT)

CIC subduction zone lengths exhibit ephemeral mid- to long-wavelength periodicities that appear to dominate for prolonged time intervals, yet are completely absent in other intervals. The most significant periodic component in the 24-48 Myr band exists 300-350 Ma, returning 225-125 Ma and transitioning into the 48-60 Myr band between 150 and 100 Ma (Fig. 2a). In contrast, there are broad regions where signals of mid- to long-wavelength components remain strong in the non-CIC subduction zone length data (Fig. 2b). Notably, the strongest significant signal components are in the 48-96 Myr band and the 24-32 Myr band over a similar time period (325-125 Ma), demarcating a broad region of power where, conversely, there is distinctly no signal component in the CIC subduction zone length signal (Fig. 2a). At certain time periods the 10-18 Myr signal component in non-CIC subduction zone lengths becomes

significant, which is not identifiable in CIC subduction zone data. Total global subduction zone lengths have several clear and persistent signals through time, primarily in the 24-32 Myr, 48-64 Myr and 100-128 Myr waveband (Fig. 2c). However, the long-term, 100-128 Myr periodicity is not well localised in time as much of the result lies outside the COI. Intermittent, sporadic regions of short- to mid-wavelength signal components appear in the proxy-CO_2 record, with the highest peaks within a confidence level of 95% occurring between 350 to 250 Ma (Fig. 2d). During this time period, a prominent peak of ~32 Myr cycles appears, transitioning into a broader 12-36 Myr band between 300 and 250 Ma (Fig. 2c). There is very little overlap in oscillatory behaviour between the subduction zone length results and the proxy-CO_2 record.

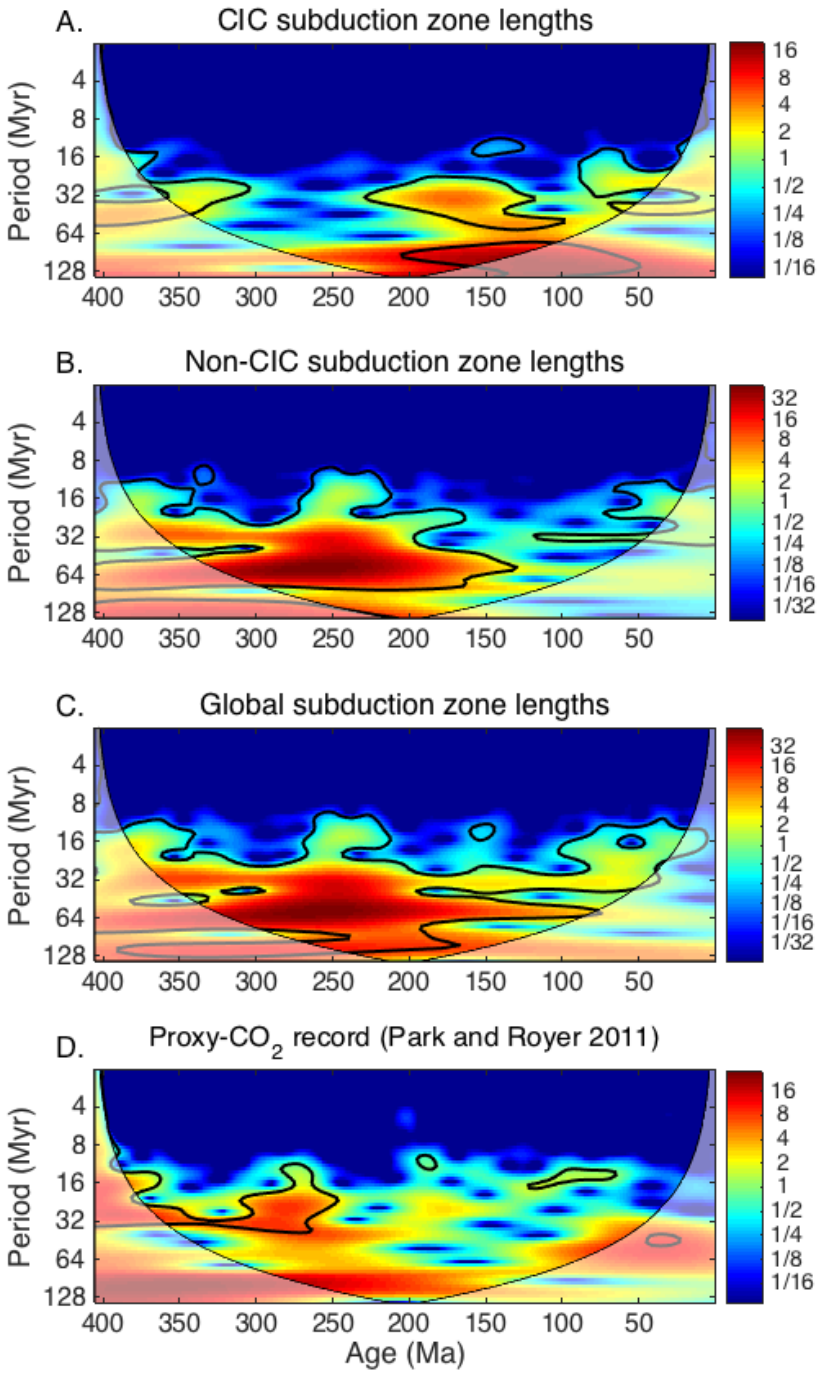
A.
CIC subduction zone lengths
Period (Myr)
4
8
16
32
64
128
400
350
300
250
200
150
100
50
16
8
4
2
1
1/2
1/4
1/8
1/16
B.
Non-CIC subduction zone lengths
Period (Myr)
4
8
16
32
64
128
400
350
300
250
200
150
100
50
32
16
8
4
2
1
1/2
1/4
1/8
1/16
1/32
C.
Global subduction zone lengths
Period (Myr)
4
8
16
32
64
128
400
350
300
250
200
150
100
50
32
16
8
4
2
1
1/2
1/4
1/8
1/16
1/32
D.
Proxy-CO2 record (Park and Royer 2011)
Period (Myr)
4
8
16
32
64
128
400
350
300
250
200
150
100
50
Age (Ma)
16
8
4
2
1
1/2
1/4
1/8
1/16

Figure 2: Continuous wavelet transforms (CWT) for (a) CIC and (b) non-CIC, (c) global subduction zone lengths and (d) the proxy-CO_2 data from Park and Royer (2011). Thick black contours designate the 5% significance level against a red noise background spectrum. The cone of influence (white translucent region) is where edge effects distort the spectrum. The colour bar indicates the wavelet power, with hotter colours corresponding to the maxima. Note the logarithmic scale of the Period (Myr) axis.

4.2 Cross-wavelet Transform (XWT) and wavelet coherence (WTC)

The periodic terms common in the subduction zone length time series and the proxy-CO_2 record were investigated further using XWT and WTC (Fig. 3). Generally, the WTC analysis between subduction zone lengths and the proxy-CO_2 record do not highlight significant nor prolonged coherence through time. While many intervals of high joint power in the XWT spectra between CIC subduction zone lengths and proxy-CO_2 trends are exhibited, primarily in the 24-48 Myr waveband (Fig. 3a), only the interval from 75-0 Ma is confirmed by WTC as being coherent through time, although the majority of the significant region lies outside the COI and thus is not localised in time (Fig. 3d). In this interval, phase-locked arrows pointing north indicate that CIC subduction zone activity precedes peaks in palaeo-atmospheric CO_2 by close to 90º in the ~40 Myr waveband. The WTC confirms the significance of high-cross amplitudes in other regions as well (380-320 Ma and 200-180 Ma), however phase arrows show that CIC lengths lag CO_2 peaks by approximately -60º (2-4 Myrs), indicating anti-correlated behaviour (Fig. 3d).

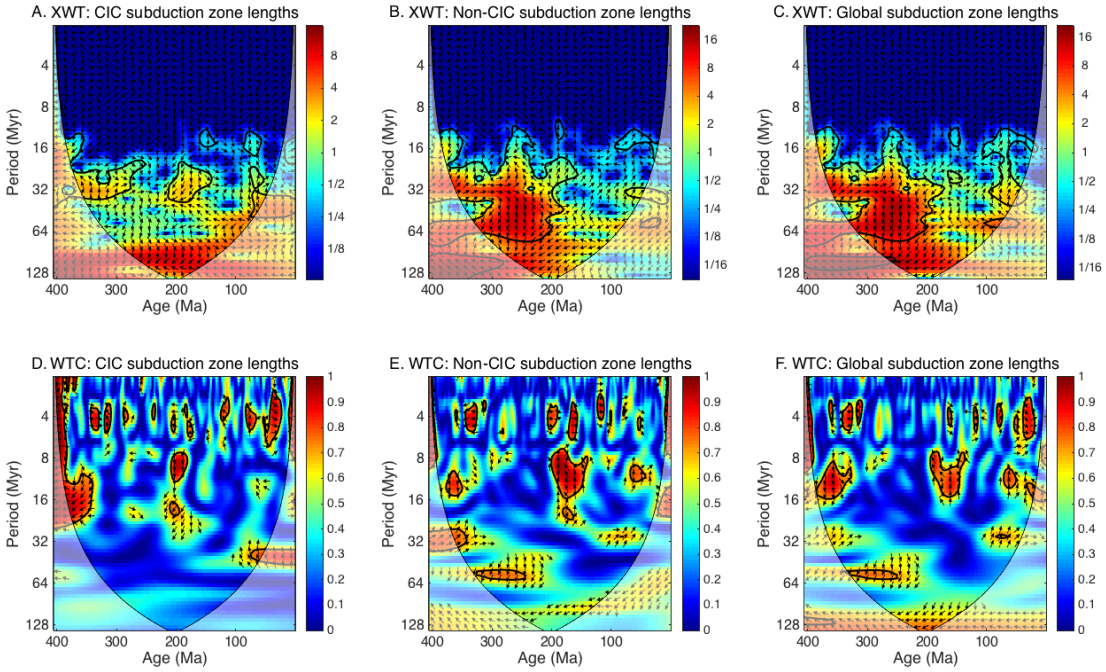

Figure 3: The cross-wavelet transforms (XWT) (top) and wavelet coherence (WTC) (bottom) for (a,d) CIC, (b,e) non-CIC and (c,f) total global subduction zone lengths respectively and the proxy-CO_2 record (Park and Royer 2011). Thick black contours designate the 5% significance level against a red noise spectrum. The white translucent region designates the cone of influence (COI). The colour bar indicates the magnitude of cross-spectral power for the XWT, and for the WTC it represents the significance level of the Monte-Carlo test. The arrows indicate the phase relationship of the two time series in time-frequency space, where east-pointing arrows indicate in-phase behaviour, west-pointing arrows indicate anti-phase behaviour, north-pointing arrows indicate that the peaks in subduction zone lengths leads the CO_2 peaks and south-pointing arrows indicating that CO_2 peaks lead peaks in subduction zone lengths.

Peaks in non-CIC subduction zone lengths also shares high joint power with proxy-CO_2 peaks at similar intervals to CIC subduction zones in the 20-48 Myr band, but in contrast shows very high joint power between 275-200 Ma where CIC subduction zone peaks do not (Fig. 3b). In the longer-wavelength band (40-80 Myr) between 300-200 Ma, high joint power exists between non-CIC subduction zone lengths and proxy-CO_2 peaks; a trend not exhibited in CIC subduction zone activity (Figs. 3b, 3a). While this timeframe is coherent, it exhibits anti-correlated phase behaviour (Fig. 3e). Only a few significant areas of the XWT between non-CIC subduction zones and proxy-CO_2 data is confirmed by wavelet coherence above the 95% confidence level. Some of these areas are common for both CIC and non-CIC subduction zone lengths (360-340 Ma and ~200-180 Ma) (Figs. 3d, 3e). Of these intervals, phase arrows in the 200-180 Ma interval in the 10-24 Myr waveband show synchronised phase behaviour indicated by north-

pointing arrows (Fig. 3e). In the 10-16 Myr waveband between 360-340 Ma, anti-phase, negatively-correlated behaviour exists where palaeo-atmospheric CO_2 peaks lead non-CIC subduction zone lengths by approximately 90º (3-4 Myrs) (Fig. 3e). Considering the non-uniqueness problem of phase analysis, this could be interpreted as a positively correlated signal with arc activity leading palaeo-atmospheric CO_2. This trend is also exhibited between CO_2 peaks and CIC subduction zone lengths during a similar time interval (Fig. 3d). The XWT and WTC for proxy-CO_2 correlations with total subduction zone lengths exhibit similar results to non-CIC subduction zone lengths (Figs. 3e, 3f), particularly regarding phase-locked behaviour in the 10-16 Myr waveband range between 375-350 Ma and 200-180 Ma (Figs. 3e, 3f). Coherence in the 30-32 Myr waveband becomes dominant between 90-70 Ma, where phase relationships in this interval indicate that in-phase CO_2 peaks are leading by ~60º (~5 Myrs) (Fig. 3f). In-phase, coherent oscillatory behaviour at this time is also present between CO_2 peaks and CIC subduction zone lengths (Fig. 3d).

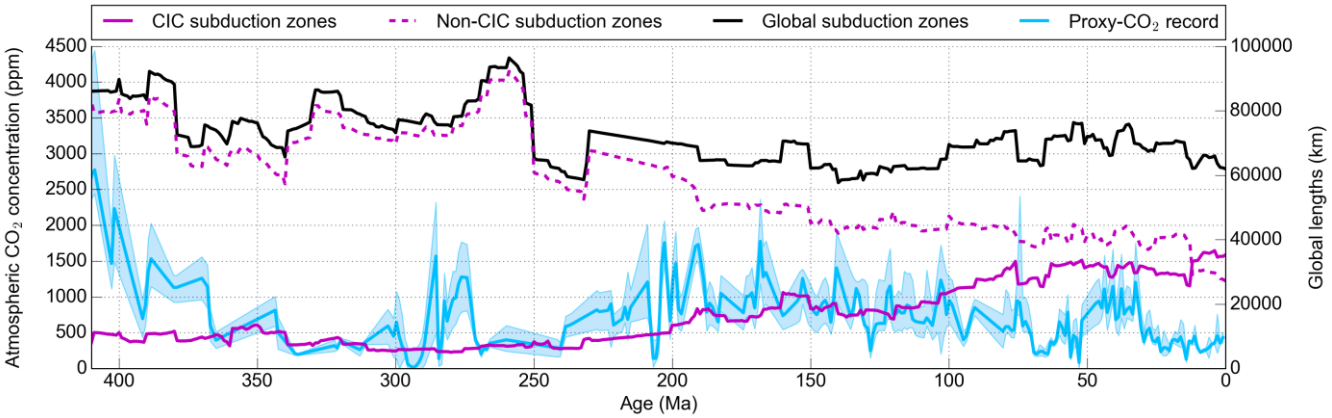

Figure 4: Total global lengths of subduction zones (black) compared with lengths of all subduction zones that intersect with buried crustal carbonate platforms (magenta, solid) and those lengths that do not intersect crustal carbonate platforms (magenta, dashed). The proxy-CO_2 record (blue line) from Park and Royer (2011) with upper and lower bounds (blue envelope**)** are displayed for comparison**.**

4.3 Comparing carbonate-intersecting arc length and palaeo-CO_2 trends

Coherence analysis suggests that CIC subduction zone lengths and palaeo-atmospheric CO_2 peaks may not be well correlated prior to 100 Ma. Indeed, CIC subduction zone lengths make up a small proportion

of global subduction zones prior to 200 Ma, beginning at 7940 km at 410 Ma and increasing to over 15 000 km only after 200 Ma (Fig. 4). However, during some time windows, periodic behaviour may be correlated. These three areas of significance highlighted by the XWT and WTC analysis are between 380-320 Ma, 210-180 Ma and 75-50 Ma (Fig. 3). Between 380 and 320 Ma, coherence analysis highlights possible in-phase 30-32 Myr linked periodic behaviour for both global and non-CIC subduction zone lengths with CO_2 peaks, which is validated by trend data (Fig. 3d). Over the period 380-340, decreasing non-CIC and global subduction zone lengths mirror the CO_2 record trend as lengths drop from ~77 000 km to ~54 000 km and ~88 000 km to ~66 000 km respectively (Fig. 4). In contrast, wavelet analysis found anti-correlated behaviour between CIC subduction zone lengths and the CO_2 record (Fig. 3d), and in line with the analysis, CIC subduction zone lengths remain relatively low (7 000-12 000 km) over this period (Fig. 4). It is evident that the magnitude of change in CIC subduction zone lengths cannot explain the precipitous drop in palaeo-atmospheric CO_2 (2 750 ppm to 200 ppm) taking place from ~410 Ma to ~340 Ma (Fig. 4).

During the 210-190 Ma interval, we observe a rapid reduction in non-CIC subduction zone lengths (~61 000 to 48 000km) and global subduction zones (~ 71 000 to 65 000 km) simultaneously with a relatively dramatic increase CIC subduction zone lengths (~10 000 to ~17 000 km) (Fig. 4). Short-wavelength periodic behaviour (~10 Myrs) exists for palaeo-CO_2 but and mid- to long-wavelength behaviour for CIC and non-CIC subduction zone lengths, which implies a scale mismatch evidenced by CWT analyses (Fig. 2). Hence, neither CIC, non-CIC nor global subduction zone lengths can adequately explain large-amplitude (~45 to 1 800 ppm), high-frequency (~10 Myr) fluctuations in palaeo-atmospheric CO_2 levels over the 210-190 Ma timeframe (Fig. 4). Between 75-0 Ma, XWT and WTC analysis highlighted a significant domain of high coherence between CIC subduction zone length data and the proxy-CO_2 record in the 40-48 Myr waveband with an arc-leading relationship of ~10 Myrs (Figs. 3a, 3d). Over the same time interval, an area of high coherence with arc-leading relationships occurs in the ~32 Myr waveband between global subduction zone lengths and the proxy-CO_2 record (Figs. 3c, 3f). This result is reflected in trend data, where both CIC and global subduction zone lengths reach a local maximum at ~75 Ma (~26 000 km and ~74 000 km respectively), drop sharply for a period of ~10 Myrs before recovering between 63 and 50 Ma (on average ~32 000 and ~72 000 km in length, respectively)

(Fig. 4). The proxy-CO_2 data mirror this decline-and-recovery trend, as palaeo-atmospheric CO_2 levels decline substantially between 75 and 70 Ma (~1200 ppm to ~250 ppm) and recover after 60 Ma (~700 ppm) (Fig. 4). Non-CIC-CO_2 XWT results highlight significant joint power during the same interval, but it was not confirmed as coherent behaviour by the WTC (Fig. 3b, 3d). In accordance, non-CIC subduction zone lengths do not sustain the same linked behaviour as CIC and global subduction zone lengths over this interval.

5 Discussion

From 250 Ma, accumulated carbonate platforms consistently intersect ~ 70% of total global subduction zone lengths (Fig. 4). Given this significant effect, we would expect that the growing reservoir of carbonate platforms would result in linked, periodic behaviour in the more recent past compared to 400-250 Ma if the length of CIC subduction zones had a dominant climate-forcing effect. CIC subduction zone lengths and the proxy-CO_2 record are largely independent with no strong leader relationship that is consistent through time, with the exception of the most recent ~75 Myr. Ultimately, our study does not support the hypothesis that carbonate-intersecting arcs have had a sustained and dominant influence on atmospheric CO_2 levels over the past 410 Myr. Instead, carbonate-intersecting subduction-derived magmatism is likely to have episodic control on atmospheric CO_2, perhaps related to the inception or abandonment of major regional continental subduction zones. However, potential issues with the large uncertainties in the proxy record, complexities in reconstructing pre-Pangea subduction zones and carbonate platforms, as well as the requirement to filter the time series may influence this result.

At present day, our estimates of CIC and global subduction zone lengths reach approximately 35 000 km and 62 000 km respectively. Recent calculations of global continental arc lengths by Cao et al. (2017) are approximately 15 000 km, which are more than half of our calculations for CIC subduction zone lengths only. Cao et al. (2017) are focussed on measuring the extent of continental volcanic arcs, whereas our investigation encompasses the total segment lengths of all subduction zones, including those that intersect carbonate platforms. Therefore, our analysis tends to capture a broader range of CO_2 degassing mechanisms along subduction zones, including diffuse outgassing from fore-arcs, back-arcs and volcanic arcs along faults, fractures and fissures, in addition to arc volcanoes. This is because melt is ubiquitous

along subduction zones, and there is very little carbon storage along arcs (Keleman and Manning, 2015). For this reason, our approach differs from that of Cao et al. (2017), as we are attempting to capture additional mechanisms of CO_2 escape along continental subduction zones, as opposed to only those directly associated with volcanic arcs, and our estimates may be regarded as an upper bound on total CO_2 emissions at subduction zones.

Wavelet analysis highlights many intervals of significant and high joint power in all XWT spectra, yet they were not coherent and thus could not be distinguished from coincidence, such as the region of high power in ~10-64 Myr wavebands from 300-200 Ma for non-CIC and global subduction zone lengths (Figs. 3b, 3c). In some intervals, wavelet analysis highlights the opposite of climate-forcing behaviour between CIC subduction zone lengths and palaeo-atmospheric CO_2 levels (i.e. where CO_2 peaks precede subduction zone lengths), such as between 210 and 190 Ma (Fig. 3a). Similarly, a long-lived coherent ~64 Myr signal in both the non-CIC subduction zone lengths and global subduction zone lengths was found to be a significantly coherent signal at the 95% level (Figs. 3e, 3f), yet the CO_2 peak occurred ~16 Myrs prior to non-CIC and global subduction length peaks and the result was not found to be meaningful in the context of climate-forcing behaviour (Fig. 4). A 30-32 Myr periodicity in the non-CIC subduction zone length signal in the 375-350 Ma interval may be interpreted as being linked to a concomitant decline in palaeo-atmospheric CO_2, a relationship which was similar in the global subduction zone lengths signal yet was insignificant at the 95% level. Both palaeobotanical and modelling investigations suggest that the rise of vascular land plants (Algeo et al., 1995) and heightened chemical weathering (Berner and Kothavala, 2001) were the dominant forces controlling the large reduction in atmospheric CO_2 during the Late Devonian, however, this result does not preclude the notion that waning CIC subduction zone lengths may have partially contributed to the cooler background climate. Our results suggest that subduction zone lengths have not consistently modulated the CO_2-forced transitions between warmer and cooler climates throughout the Phanerozoic. However similar trends in CIC subduction zone lengths and global subduction zone lengths between 75-50 Ma suggest that the Late Cretaceous to early Palaeogene warm climate may be a phenomenon forced by global subduction zone lengths rather than CIC subduction zone lengths alone.

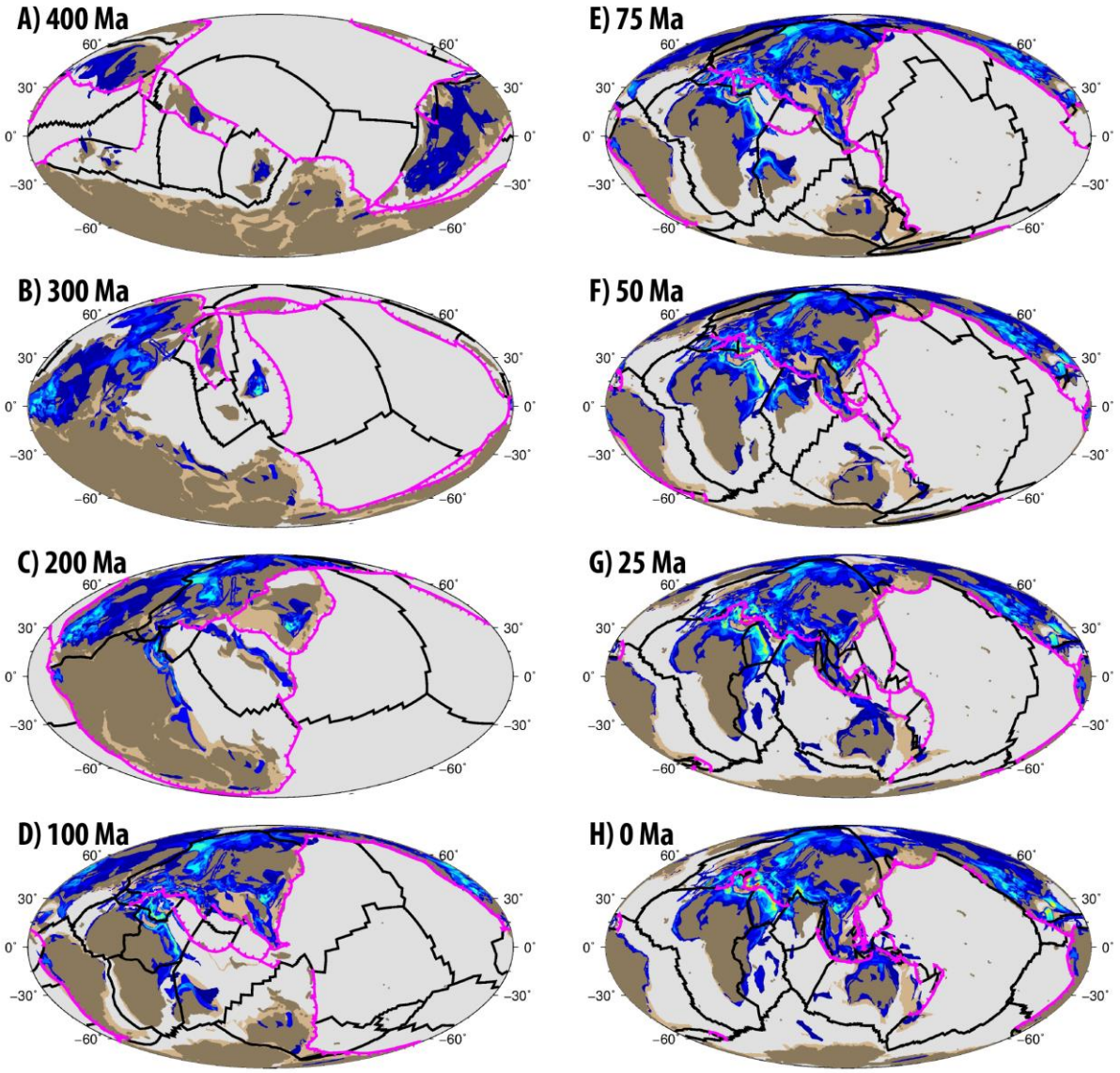

Figure 5: Plate reconstructions with plate boundaries (black), subduction zones (purple) and distributions of carbonate platforms. Carbonate platforms are distributed according to the Accumulation Model at key intervals from 400 Ma to present day. Colour bar corresponds to the duration of time that the carbonate platforms were actively developing for in the crust.

5

5.1 Implications for Late Cretaceous to Early Palaeogene Climate

Only during the most recent 75 Myrs is it plausible that CIC subduction zone lengths influenced atmospheric CO_2 based on our analysis, yet there are two factors that prevent us from viewing these correlations as causative. Firstly, while the ~32 Myr cyclicity is coherent and significant at the 5% level, it is not time-localised between 60-0 Ma as the result lies outside the COI. Secondly, CIC subduction zone length trends passively mirror total global subduction zone lengths during this time, suggesting that it is not specifically the CO_2 liberated at CIC subduction zones that drove atmospheric CO_2 peaks, but net global CO_2 emissions along subduction zones. However, the period between 75-50 Ma seems to be distinct from other times as a significant coherency occurs. The changing distribution of CIC subduction zone lengths and subduction zones between 75 and 50 Ma may have contributed to the well-studied greenhouse climate 51-53 Ma, known as the Early Eocene climatic optimum (EECO), where temperatures were about 14 ± 3ºC warmer than the pre-industrial period (Caballero and Huber, 2013). While climate interactions and feedbacks leading to the greenhouse state remain uncertain, climate sensitivity to CO_2 forcing is likely (Anagnostou et al., 2016).

According to the Accumulation model, the dramatic change that characterised the reduction in CIC subduction zone lengths ~75 Ma included the termination of a ~3 000-km-long section of a north-dipping intra-oceanic subduction zone in the Northern Tethys ocean, corresponding to the Trans-Tethyan Subduction System (Jagoutz et al., 2016), and the cessation of subduction along the Sundaland margin (McCourt et al., 1996; Zahirovic et al., 2016) (Figs. 5d, 5e). The intra-oceanic subduction in the Neo-Tethys in our model would not be classified as a carbonate-intersecting subduction zone due to the overriding plate (in this case largely oceanic lithosphere) lacking extensive carbonate platforms. In any case, this intra-oceanic subduction zone in the Accumulation Model corresponds to the emplacement of the peri-Arabian ophiolite belt along the Afro-Arabian continental margin between 80-70 Ma rather than an Andean-style arc, the erosion of which has been posited as a cause of global cooling following the EECO (Jagoutz et al., 2016) (Figs. 5d, 5e). We can therefore rule out subduction-zone-related volcanism in this region as a contributor to high CO_2 levels given that the shut-down of this arc is not associated with the cessation of Andean-style subduction.

The termination of arc volcanism particularly along the Sundaland margin, where a large area of carbonate platforms are buried, contributed ~3 000 km to the global reduction in CIC subduction zone lengths by ~7 000 km between 75-65 Ma (Figs. 5e, 5f). The resumption of subduction along the Sunda-Java trench at 65 Ma in the model as well as the emplacement of a set of carbonate platforms in the lower latitudes at 63 Ma explain the modelled results of an increase in CIC subduction zone lengths at 63 Ma which persist past 50 Ma (Fig. 5f). The EECO occurred approximately 10 Myr later, supporting the 10 Myr lag in peaks of a ~40 Myr periodicity found by the CIC-proxy-CO_2 XWT and WTC (Fig. 3a). Our analysis shows a concomitant increase in non-CIC subduction zone lengths (Fig. 4), but the periodic behaviour was not found to be significantly coherent and so coincidental peaks cannot be ruled out. Modern volcanic CO_2 output from arcs in Indonesia, Papua New Guinea, parts of the Andes and Italian Magmatic Province are strongly influenced by carbonate assimilation (Mason et al., 2017) and volcanoes in those regions currently contribute significantly to global atmospheric CO_2 flux (Carter and Dasgupta, 2015). Assuming a similar subduction style, this result gives plausibility to the idea that volcanic activity along the Sunda-Java trench during the Cretaceous was also significantly contributing to global CO_2 output.

Previous studies have suggested that global arc CO_2 contributed to the baseline warm climate of the Late Cretaceous and late Palaeogene, due to the greater size of carbonate reservoirs in continents and the increased continental arc lengths (Lee et al., 2013; Carter and Dasgupta, 2015; McKenzie et al., 2016; Cao et al., 2017). Our results agree well with the hypothesis, as a relative increase in CIC subduction zone lengths has been linked to a peak in atmospheric CO_2 from 75-50 Ma, contributing to enhanced CO_2 degassing. However, it cannot be determined from this study whether the increase in global subduction zone lengths is more important than the relative increase in the lengths that intersect carbonate platforms.

5.2 Limitations of wavelet analysis

Wavelet analysis is inherently sensitive to the shape of signals, and as such, adjustment of filtering and processing techniques introduces variations in the results. Firstly, the proxy-CO_2 signal applied here is a mean signal between reported standard deviations on proxy data (Park and Royer, 2011). While the uncertainties appear to be time-localised, the uncertainty in CO_2 concentrations in the proxy record could not be captured by our method of extracting only one signal. Moreover, the choice of interpolation method

of the proxy-CO_2 record may subdue actual oscillations in the signal, affecting phase relationships and confidence intervals. Similarly, a size-7 moving average window filter was chosen to remove high-frequency noise, yet it may have moved trends forward in time, which ultimately changes whether peaks overlap or not and adds uncertainty to results. Peaks in the XWT were robust in that they were found to appear in XWT plots regardless of the intensity of smoothing, yet the significance contours differed strongly due to smoothing. For instance, with a longer low-bandpass filter, small-scale oscillations <5 Myrs were removed, reducing areas of significant power in the shorter wavebands. Similarly, when experimenting with a high-bandpass filter, significant regions were directed away from the longer periodicities of >64 Myrs to shorter periodicities. The low-bandpass filter was chosen to remove the noise for smaller periodicities where fluctuations were less likely to represent trends and more likely to represent artefacts of interpolation, yet this measure erases the fidelity of short-term oscillations in the time series. Hence detail on the <10 Myr scale is not adequately represented, and thus our study was unable to evaluate short-term relationships.

Our analysis technique cannot quantify the error that propagates from uncertainty in the proxy-CO_2 record and subduction zone length signal through to the correlation uncertainty. Interpolation and filtering of the proxy-CO_2 record necessarily cannot account for the uncertainty displayed by the envelope as only one signal can be extracted. Similarly, the Matthews et al. (2016) tectonic plate model represents one interpretation of geological data which becomes sparse for deeper geological time, especially for pre-Pangea times (before ~250-200 Ma). The nature of using a tectonic framework means only one subduction zone length signal can be extracted from the model, which does not lend well to estimations of error. In this way, the selection and comparison of two signals with large uncertainty are not sufficient in eliciting well-constrained periodic behaviour and true correlations.

XWT analysis describes areas with high power which can be misleading when the XWT spectrum is not normalised. For instance, areas of high joint power were found where relatively flat peaks in the CIC subduction zone length data occurred simply because of the large amplitude of peaks in the proxy-CO_2 data. The vast differences in magnitude do not necessarily constitute a causative relationship. WTC analysis does not present this problem because the spectrum is normalised, and hence periodicities with strong power were not necessarily found to be coherent (Maraun and Kurths, 2004). The combination of

both measures somewhat circumvents the problem of misleading peaks in the XWT, but not all. Given that wavelet analysis is very sensitive to magnitude and timing of peaks, the fact that the uncertainty in our modelled estimates of subduction zone lengths are not well-constrained introduces variability in correlative relationships. Wavelet analysis, like other signal processing techniques, is limited by the length of the time series data investigated. Periods of greater than half the time series length cannot be examined using this method (Winder, 2002). Therefore, very-long oscillations on the scale of 250 Myr or more could not be derived from our data. One reason for examining patterns on 250 Ma periods is due to the very-long-term nature of supercontinent cycles. The accretion of supercontinents such as Pangea and Rodinia are associated with shortened continental subduction zone lengths, whilst continental break-up and dispersal initiates subduction on the edges of continents, and thus increases continental subduction zone lengths (Donnadieu et al., 2004; Lenardic et al. 2011; Lee et al., 2016). These changing modes of supercontinent break-up or accretion have the potential to influence climate. Given that supercontinent cycles exceed 200 Myr in length and exert a large effect on the length of continental arcs (Lee et al., 2013), applying this analysis to plate reconstructions that capture multiple supercontinent cycles (e.g. Merdith et al., 2017) to investigate whether such long-term linkages exist between atmospheric CO_2 and global subduction zone emissions.

5.3 Limitations of model assumptions

The extent to which our models are representative of subduction zone CO_2 emissions is limited by some issues with the subduction zone quantification approach. The subduction zone modelling attempted to approximate atmospheric CO_2 flux at subduction zones without directly measuring it by assuming a constant CO_2 flux and a unit-correspondence of subduction zone lengths to volcanoes, vents or fissures. Both assumptions are problematic. There are several dynamic factors that govern subduction-zone-CO_2 flux such as convergence rates (van der Meer et al., 2014), the composition and volume of subducted sediments (Rea and Ruff, 1996), convergence obliquity (Kerrick and Connolly, 2001), slab volume flux (Fischer, 2008), the relative contribution of metamorphic decarbonation in the crust and in the mantle wedge (Keleman and Manning, 2015) and the efficiency of decarbonation (Johnston et al., 2011). The model does not account for these factors and assumes that the parameters of CO_2 flux have remained

constant in time. In addition, the number of volcanoes or vents per unit length of subduction zones is neither constant through time nor correlated, at least for the circum-Pacific arc and Central American arc (Kerrick, 2001). Furthermore, the Accumulation Model has no way to account for carbonate platform thicknesses, and thus cannot account for the realistic depletion of crustal carbonate reservoirs through time. The inability of the model to incorporate the complexity of depleting carbonate platforms may lead to sampling bias during continental collisions. This highlights an area of future improvement, including the utilisation of subduction zone geodynamic-geochemical modelling (e.g. Gonzales et al., 2016) by tracking different CO_2 reservoirs in a geodynamic context.

Furthermore, uncertainty cannot be measured using our GPlates modelling approach. Uncertainty propagates through the plate motion model over deeper reaches of geological time, such that it is impossible to quantify uncertainty of all possible configurations of subduction zones, especially in the pre-Pangea timeframe. Moreover, there is a much greater uncertainty in the dynamic mechanisms of carbon cycling along subduction zones, and quantification of all geochemical decarbonation reactions is still in infancy (Gonzales et al., 2016). For these reasons, formal uncertainties cannot yet be quantified for models of subduction zone carbon cycling. Taking all limitations into consideration, the Accumulation Model still provides a first-order approximation of changing subduction zone lengths through time and the interaction with (buried) carbonate platforms as an indicator of CO_2 degassing, especially for the Late Cretaceous and early Paleogene.

6 Conclusions

Wavelet analysis is a useful tool in elucidating coherent, phase-related periodicities between the CO_2 record and various climate forcing factors. Our analysis has revealed that CIC subduction zone activity is largely independent to the proxy-CO_2 record over the past 410 Myr except for the period 75-50 Ma. The CIC subduction zone lengths that we derived from an Accumulation model of carbonate platform evolution do not find reasonable and persistent periodicities that explain atmospheric CO_2 flux, however there may be some causal relationships in the Late Cretaceous to early Palaeogene that are supported by previous modelling efforts.

This analysis lends partial support to the idea that, at certain times, carbonate-intersecting subduction zone activity is more important than non-carbonate intersecting activity in driving atmospheric CO_2, yet the climate system is vastly complex and the result could mean that other processes have dominated climate feedback mechanisms through time, such as the proliferation of terrestrial plant life (Algeo et al., 1995), silicate weathering (Kent and Muttoni, 2008) and the emplacement of large igneous provinces (Belcher and Mander, 2012).

Generally, an absence of constraints on carbon-climate interactions in deep-time makes it difficult to test hypotheses about greenhouse and icehouse climate states. Clearly, more robust reconstructions of climate-forcing processes are needed to improve our understanding of the deep carbon system. It is suggested that further investigations be carried out at specific time intervals to eliminate the uncertainty around the time periods within the COI at the end of the data series (between 410-350 Ma and 50-0 Ma). With adjustments to the parameters and assumptions governing the carbonate platform evolution models, the data can be used as input into fully-coupled planetary-scale climate and carbon cycle box models. This would provide the most comprehensive and self-consistent approach to understand the contribution of emissions at subduction zones to the deep carbon cycle.

Code and data availability

The subduction zone toolkit by Doss et al. (2016) was developed as a product of this research and has been made publicly available for use with open-source plate reconstruction software, GPlates. The toolkit includes all proxy CO_2 data, pyGPlates and bash scripts as well as the Matthews et al. (2016) plate model. Both the Signal Processing Toolbox™ and Wavelet Coherence Toolbox™ for MATLAB® were used in analysis and the production of figures. The Wavelet Coherence Toolbox™ can be found at http://noc.ac.uk/marine-data-products/cross-wavelet-wavelet-coherence-toolbox-matlab, while the Signal Processing Toolbox™ can be found at http://au.mathworks.com/help/signal/index.html.

Doss, S., Zahirovic, S., Müller, D. and Pall, J: DCO Modelling of Deep Time Atmospheric Carbon Flux from Subduction One Interactions: Plate Models & Minor Edits, Zenodo, http://dx.doi.org/10.5281/zenodo.154001, 2016.

Author Contribution

Sebastiano Doss and Jodie Pall developed the Subduction Zone toolkit together and carried out modelling experiments under the supervision of Dietmar Müller and Sabin Zahirovic. Figures were prepared by Jodie Pall and Sebastiano Doss, and the toolkit repository was prepared by Sebastiano Doss. Jodie Pall conducted wavelet analysis with assistance from Rakib Hassan. Jodie Pall also prepared the manuscript with contributions from all co-authors.

Competing interests

The authors declare that they have no conflict of interest.

Acknowledgements

The authors acknowledge and thank the Alfred P Sloan Foundation and the Deep Carbon Observatory (DCO) for funding this research. We would also like to thank members of the EarthByte Group for all their assistance, as well as the University of Sydney for supporting open source and open access research.

References

Algeo, T.J., Berner, R.A., Maynard, J.B. and Schekler, S.E.: Late Devonian oceanic anoxic events and biotic crises: "Rooted" in the evolution of vascular land plants?, GSA Today, 5, 64-66, 1995.

Anagnostou, E., John, E. H., Edgar, K. M., Foster, G. L., Ridgwell, A., Inglis, G. N., Pancost, R.D., Lunt, D.J., Pearson, P. N.: Changing atmospheric CO2 concentration was the primary driver of early Cenozoic climate, Nature, 533,7603, 380-384, 2016.

Belcher, C. M., and Mander, L.: Catastrophe: Extraterrestrial impacts, massive volcanism, and the biosphere, in The Future of the World's Climate, edited by A. Henderson-Sellers and K. McGruffie, 463–485, Elsevier, Amsterdam, 2012.

Berner, R. A., and Caldeira, K.: The need for Mass balance and feedback in the geochemical carbon cycle, Geology, 25, 955-956, 1997.

Berner, R. A., and Kothavala, Z.: GEOCARB III: a revised model of atmospheric CO2 over Phanerozoic time, American Journal of Science, 301, 182-204, 2001.

Berner, R. A.: The Phanerozoic Carbon Cycle: CO2 and O2, Oxford University Press, 2004.

Berner, R.A.: GEOCARBSULF: A combined model for Phanerozoic atmospheric O2 and CO2, Geochimica et Cosmochimica Acta, 70, 23, 5653-5664, 2006.

Boyden, J. A., Müller, R. D., Gurnis, M., Torsvik, T. H., Clark, J. A., Turner, M., Ivey-Law, H., Watson, R. J., and Cannon, J. S.: Next-generation plate-tectonic reconstructions using GPlates, Geoinformatics: cyberinfrastructure for the solid earth sciences, 9, 5-114, 2011.

Burton, M. R., Sawyer, G. M., and Granieri, D.: Deep carbon emissions from volcanoes, Rev. Mineral. Geochem, 75, 323-354, 2013.

Caballero, R., and Huber, M.: State-dependent climate sensitivity in past warm climates and its implications for future climate projections, Proceedings of the National Academy of Sciences, 110, 14162-14167, 2013.

Cao, W., Lee, C-T. A., Lackey, J.S.: Episodic nature of continental arc activity since 750 Ma: A global compilation, Earth and Planetary Science Letters, 461, 85-95, 2016.

Carter, L. B., and Dasgupta, R.: Hydrous basalt–limestone interaction at crustal conditions: Implications for generation of ultracalcic melts and outflux of CO 2 at volcanic arcs, Earth and Planetary Science Letters, 427, 202-214, 2015.

Cohen, K., Finney, S., Gibbard, P., and Fan, J.-X.: The ICS international chronostratigraphic chart, Episodes, 36, 199-204, 2013.

Domeier, M., and Torsvik, T. H.: Plate tectonics in the late Palaeozoic, Geoscience Frontiers, 5, 303-350, 2014.

Doss, S., Zahirovic, S., Müller, D. and Pall, J.: DCO Modelling Of Deep Time Atmospheric Carbon Flux from Subduction Zone Interactions: Plate Models and Minor Edits, http://doi.org/10.5281/zenodo.154001, 2016.

EarthByte Group: GPlates 1.5, Sydney, Australia http://www.gplates.org/download.html, 2015.

ESRI: Release 10, Documentation Manual. Redlands, CA, Environmental Systems Research Institute, 2011.

Fischer, T. P.: Fluxes of volatiles (H2O, CO2, N2, Cl, F) from arc volcanoes, Geochemical Journal, 42, 21-38, 2008.

Golonka, J. and Kiessling, W.: Phanerozoic time scale and definition of time slices, in: Phanerozoic Reef Patterns, Kiessling, W., Flugel, E. and Golonka, J. (eds), SEPM (Society for Sedimentary Geology) Special Publication 72, 11-29, 2002.

Gonzalez, C., Gorczyk, W., and Gerya, T.: Decarbonation of subducting slabs: Insight from petrological–thermomechanical modeling, Gondwana Research, 36, 314-332, 2016.

Grinsted, A., Moore, J. C., and Jevrejeva, S.: Application of the cross wavelet transform and wavelet coherence to geophysical time series, Nonlinear processes in geophysics, 11, 561-566, 2004.

Grotzinger, J. P., and James, N. P.: Precambrian carbonates: evolution of understanding, SEPM Special Publication 6, 3-20, 2000.

Gurnis, M., Turner, M., Zahirovic, S., DiCaprio, L., Spasojevic, S., Müller, R., Boyden, J., Seton, M., Manea, V., and Bower, D.: Plate Tectonic Reconstructions with Continuously Closing Plates, Computers & Geosciences, 38, 35-42, 2012.

IPCC: Climate Change 2013: The Physical Science Basis. Contribution of Working Group I to the Fifth Assessment Report of the Intergovernmental Panel on Climate Change, Cambridge University Press, Cambridge, United Kingdom and New York, NY, USA, 1535 pp., 2013.

Jagoutz, O., Macdonald, F. A., and Royden, L.: Low-latitude arc–continent collision as a driver for global cooling, Proceedings of the National Academy of Sciences, 113, 4935-4940, 2016.

Johnston, F. K., Turchyn, A. V., and Edmonds, M.: Decarbonation efficiency in subduction zones: Implications for warm Cretaceous climates, Earth and Planetary Science Letters, 303, 143-152, 2011.

Keleman, P., and Manning, C.: Reevaluating carbon fluxes in subduction zones, what goes down, mostly comes up. PNAS 112, E3997–E4006, 2015.

Kent, D. V., and Muttoni, G.: Equatorial convergence of India and early Cenozoic climate trends, Proceedings of the National Academy of Sciences, 105, 16065-16070, 2008.

Kent, D. V., and Muttoni, G.: Modulation of Late Cretaceous and Cenozoic climate by variable drawdown of atmospheric pCO 2 from weathering of basaltic provinces on continents drifting through the equatorial humid belt, Climate of the Past, 9, 525-546, 2013.

Kerrick, D. M.: Present and past nonanthropogenic CO2 degassing from the solid Earth, Reviews of Geophysics, 39, 565-585, 2001.

Kerrick, D., and Connolly, J.: Metamorphic devolatilization of subducted oceanic metabasalts: implications for seismicity, arc Magmatism and volatile recycling, Earth and Planetary Science Letters, 189, 19-29, 2001.

Kiessling, W., Flügel, E., and Golonka, J.: Fluctuations in the carbonate production of Phanerozoic reefs, Geological Society, London, Special Publications, 178, 191-215, 2000.

Kiessling, W., Flügel, E., and Golonka, J.: Patterns of Phanerozoic carbonate platform sedimentation, Lethaia, 36, 195-225, 2003.

Kump, L. R., Brantley, S. L., and Arthur, M. A.: Chemical weathering, atmospheric CO2, and climate, Annual Review of Earth and Planetary Sciences, 28, 611-667, 2000.

Lau, K., and Weng, H.: Climate signal detection using wavelet transform: How to make a time series sing, Bulletin of the American Meteorological Society, 76, 2391-2402, 1995.

Lee, C. T. A., Lackey, J. S.: Global continental arc flare-ups and their relation to long-term greenhouse conditions, Elements, 11,2,125-130, 2015.

Lee, C.-T. A., Shen, B., Slotnick, B. S., Liao, K., Dickens, G. R., Yokoyama, Y., Lenardic, A., Dasgupta, R., Jellinek, M., and Lackey, J. S.: Continental arc–island arc fluctuations, growth of crustal carbonates, and long-term climate change, Geosphere, 9, 21-36, 2013.

Lee, H., Muirhead, J. D., Fischer, T. P., Ebinger, C. J., Kattenhorn, S. A., Sharp, Z. D., and Kianji, G.: Massive and prolonged deep carbon emissions associated with continental rifting, Nature Geoscience, 2016.

Lenardic, A., Moresi, L., Jellinek, A., O'Neill, C., Cooper, C.M. and Lee, C.T.: Continents, supercontinents, mantle thermal mixing, and mantle thermal isolation: Theory, numerical simulations and laboratory experiments, Geochem. Geophys. Geosyst., 12, Q10016, doi:10.1029/2011GC003663, 2011.

Matthews, K. J., Maloney, K. T., Zahirovic, S., Williams, S. E., Seton, M., and Müller, R. D.: Global plate boundary evolution and kinematics since the late Palaeozoic, Global and Planetary Change, 146, 226-250, http://dx.doi.org/10.1016/j.gloplacha.2016.10.002, 2016.

McCourt, W., Crow, M., Cobbing, E., and Amin, T.: Mesozoic and Cenozoic plutonic evolution of SE Asia: evidence from Sumatra, Indonesia, Geological Society, London, Special Publications, 106,1, 321-335, 1996.

McKenzie, N. R., Horton, B. K., Loomis, S. E., Stockli, D. F., Planavsky, N. J., and Lee, C. T.: Continental arc volcanism as the principal driver of icehouse-greenhouse variability, Science (New York, N.Y.), 352, 444-447, 10.1126/science.aad5787, 2016.

Merdith, A.S., Collins, A.S., Williams, S.E., Pisarevsky, S., Foden, J.D., Archibald, D.B., Blades, M.L., Alessio, B.L., Armistead, S., Plavsa, D., Clark, C. an Muller, R.D.: A full-plate global reconstruction of Neoproterozoic, Gondwana research, 50, 84-134, 2017.

Müller, R. D., Seton, M., Zahirovic, S., Williams, S. E., Matthews, K. J., Wright, N. M., Shephard, G. E., Maloney, K., Barnett-Moore, N., and Hosseinpour, M.: Ocean basin evolution and global-scale plate reorganization events since Pangea breakup, Annual Review of Earth and Planetary Sciences, 44, 107-138, 2016.

Park, J., and Royer, D. L.: Geologic constraints on the glacial amplification of Phanerozoic climate sensitivity, American Journal of Science, 311, 1-26, 2011.

Prokoph, A., and El Bilali, H.: Cross-wavelet analysis: a tool for detection of relationships between palaeoclimate proxy records, Mathematical geosciences, 40, 575-586, 2008.

Rea, D. K., and Ruff, L. J.: Composition and Mass flux of sediment entering the world's subduction zones: implications for global sediment budgets, great earthquakes, and volcanism, Earth and Planetary Science Letters, 140, 1-12, 1996.

Ridgwell, A., and Zeebe, R.: The role of the global carbonate cycle in the regulation and evolution of the Earth system, Earth and Planetary Science Letters, 234, 299-315, 10.1016/j.epsl.2005.03.006, 2005.

Royer, D. L.: CO 2-forced climate thresholds during the Phanerozoic, Geochimica et Cosmochimica Acta, 70, 5665-5675, 2006.

Scotese, C. R.: PALAEOMAP PalaeoAtlas for GPlates and the PalaeoData Plotter Program, PALAEOMAP Project, http://www.earthbyte.org/palaeomap- palaeoatlas-for-gplates, 2016.

Siebert, L., and Simkin, T.: Volcanoes of the world: An illustrated catalog of Holocene volcanoes and their eruptions, 2014.

Seton, M., Müller, R., Zahirovic, S., Gaina, C., Torsvik, T., Shephard, G., Talsma, A., Gurnis, M., Turner, M., Maus, S., and Chandler, M.: Global continental and ocean basin reconstructions since 200 Ma, Earth-Science Reviews, 113, 212-270, 2012.

Sundquist, E. T.: Steady- and non-steady-state carbonate-silicate controls on atmospheric CO2, Quaternary Science Reviews, 10, 283-296, http://dx.doi.org/10.1016/0277-3791(91)90026-Q, 1991.

Torrence, C., and Compo, G. P.: A practical guide to wavelet analysis, Bulletin of the American Meteorological society, 79, 61-78, 1998.

van der Meer, D. G., Zeebe, R. E., van Hinsbergen, D. J., Sluijs, A., Spakman, W., and Torsvik, T. H.: Plate tectonic controls on atmospheric CO2 levels since the Triassic, Proceedings of the National Academy of Sciences, 111, 4380-4385, 2014.

Walker, J. C., Hays, P., and Kasting, J. F.: A negative feedback mechanism for the long-term stabilization of Earth's surface temperature, Journal of Geophysical Research: Oceans, 86, 9776-9782, 1981.

Wessel, P., Smith, W.H.F., Scharroo, R., Luis, J.F. and Wobbe, F.: GMT 5.2.1., SOEST, Dept. of Geology & Geophysics, Honolulu, Hawaii, http://gmt.soest.hawaii.edu/projects/gmt/wiki/Download, 2015.

Whittaker, J.M., Müller, R.D., Sdrolias, M., and Heine, C.: Sunda-Java trench kinematics, slab window formation and overriding plate deformation since the Cretaceous, Earth and Planetary Science Letters, 255, 445-457, http://dx.doi.org/10.1016/j.epsl.2006.12.031, 2007.

Winder, S.: Analog and Digital Filter Design, Elsevier Science, 2002.

Zahirovic, S., Matthews, K. J., Flament, N., Müller, R. D., Hill, K. C., Seton, M., and Gurnis, M.: Tectonic evolution and deep mantle structure of the eastern Tethys since the latest Jurassic, Earth Science Reviews, 162, 293-337, 2016.